Monitoring snow depth variations in an avalanche release area using low-cost lidar and optical sensors

Pia Ruttner[1,2,3], Annelies Voordendag[3], Thierry Hartmann[1], Julia Glaus[1,2,4], Andreas Wieser[3], and Yves Bühler[1,2]

[1]WSL Institute for Snow and Avalanche Research SLF, Davos Dorf, 7260, Switzerland
[2]Climate Change, Extremes, and Natural Hazards in Alpine Regions Research Center CERC, Davos Dorf, 7260, Switzerland
[3]Institute of Geodesy and Photogrammetry, ETH Zurich, Zurich, 8092, Switzerland
[4]Institute for Geotechnical Engineering, ETH Zurich, Zurich, 8092, Switzerland

Correspondence: Pia Ruttner (pia.ruttner@slf.ch)

Abstract. Snow avalanches threaten people and infrastructure in mountainous areas. For the assessment of temporal protection measures of infrastructure when the avalanche danger is high, local and up-to-date information from the release zones and the avalanche track is crucial. One main factor influencing the avalanche situation is wind-drifted snow, which causes variations in snow depth across a slope. We developed a monitoring system using low-cost lidar and optical sensors, to measure snow depth variations in an avalanche release area at a high spatiotemporal scale (centimeter to low decimeter spatial resolution and hourly temporal resolution). We analyze data obtained from such a monitoring system, installed within an avalanche release area at 2200 m a.s.l. close to Davos in the Swiss Alps. The system comprises two measurement stations and has been operational since November 2023. We present the experiences and insights gained from a preliminary analysis of the data obtained so far. The temporal variations of the spatial coverage show the potential and limitations of the system under varying weather conditions. A comparison of the surface elevation models derived from the lidar data and from photogrammetric processing of UAV-based images shows a good agreement, with a mean vertical difference of 0.005 m and standard deviation of 0.15 m. An avalanche event and a period of snowfall with strong winds chosen as case studies, show the potential and limitations of the proposed system to detect changes in the snow depth distribution on a low decimeter level, or better. The results obtained so far indicate that a measurement system with a few setups in or near an avalanche slope can provide information about the small scale snow depth distribution changes in near-realtime. We expect that such systems and the related data processing have the potential to support experts in their decisions on avalanche safety measures in the future.

1 Introduction

People and infrastructure in mountainous areas with seasonal snow cover face avalanche danger. There are different possibilities to mitigate the associated risks. Common routines in temporary avalanche mitigation include 1) avalanche warning, 2) closing of infrastructure e.g. roads, 3) evacuation of people, and 4) triggering small sized avalanches using explosives. Such measures have significant impact on people and their economy, so the aim is to apply such measures as precise as possible. However, local experts have in most cases limited information to base their decisions on. They mainly rely on the avalanche bulletin,

the weather forecast, automated weather stations, and most importantly, on their own intuition and experience. Among other parameters, the current snow depth distribution in the avalanche release areas would be valuable information. When snow during a snowfall event or old snow from near surface layers is redistributed by the wind, this modifies the total amount of snow available for avalanche release and changes the composition of the snowpack. The redistribution may lead to the formation of a slab (wind slab), denser than the layer below (EAWS, 2024). Soft and loose old snow beneath the wind slab often turns into a weak layer. Changes of wind speed during the redistribution can cause the formation of weak layers even within a wind slab. Observing and quantifying variations in snow depth, particularly when related to wind-driven distribution, is therefore important to capture one of the major drivers causing avalanches (Schweizer et al., 2003).

There are different methods to measure snow depths. The most traditional method is to stick a pole or stake with a scale into the snow cover and read off the snow depth, which gives a point measurement at a specific time. This type of measurement can also provide a time series, if the pole is permanently installed and a camera is set up to automatically take pictures of the pole (Garvelmann et al., 2013; Dong and Menzel, 2017; Kopp et al., 2019). Other methods for the measurement of snow depth as a time series are the use of ultrasonic sensors, often as part of automatic weather stations (Lehning et al., 1999), or GNSS reflectometry (Larson et al., 2009). However, most of these are single point measurements and do typically not reveal the variations of snow depth across a slope.

For areal acquisitions of the snow cover the most used systems are lidar (Light Detection and Ranging) sensors and photo cameras. Both systems are either used from the air or on the ground. Airborne systems have the advantages of better spatial coverage (less topographic occlusions) and potentially more favourable acquisition angles (sensing direction can be roughly orthogonal to terrain). Civilian Uncrewed Aerial Vehicles (UAVs) typically operate at low altitudes above ground (e.g., up to about 200 m). When used as a carrier platform for photo cameras or lidar sensors, they enable high spatial resolution (cm-level) (Bühler et al., 2016; Harder et al., 2016; Jacobs et al., 2021), but the area that can be covered per campaign is limited to a few square kilometers. When using airplanes (Bühler et al., 2015; Nolan et al., 2015; Bührle et al., 2023) or satellite platforms (Romanov et al., 2003; Marti et al., 2016; Shaw et al., 2020), the covered area can be much larger, but the achievable spatial resolution decreases. Due to high costs, one disadvantage of airborne systems is the limited temporal resolution. With a ground-based system that can measure (almost) continuously and autonomously, an area of interest can be acquired with higher temporal resolution, but with the drawback of having shadowing effects due to topography and often unfavourable acquisition angles (large angles between the sensor and the surface normal).

For the computation of a 3D model using photogrammetry, each point needs to be captured in at least two images from different viewpoints. This can be achieved with a setup of multiple cameras (Basnet et al., 2016; Deschamps-Berger et al., 2020; Filhol et al., 2019; Mallalieu et al., 2017) or one moving camera capturing overlapping images, (Liu et al., 2021; Bühler et al., 2015; Bührle et al., 2023; Marti et al., 2016; Shaw et al., 2020; Bernard et al., 2017). Photogrammetric approaches rely on recognizable features in the acquired images. For the application on snow it is important that the snow cover shows certain features, for example structures induced by wind, and that illumination conditions are favorable, such that those features are visible in the captured images (Bühler et al., 2016, 2017).

Lidar sensors on the other hand use an active measurement technique, where modulated light is emitted, e.g., a light pulse, the direction of emission and the time of flight until reception of the reflected light are recorded, and the position of the reflecting surface relative to the lidar sensor is calculated. Therefore, compared to photogrammetric acquisitions, lidar sensors are less dependent on the ambient light, do not require radiometric surface texture, and can also operate during the night. An important criterion for the application of lidar sensors on snow is the operating wavelength. Most available lidar sensors use a wavelength of 1550 nm, where the reflectance of snow has a local minimum. It is possible to measure snow at that wavelength, but the achievable maximum range will likely be much lower than the range specification of the sensor. The highest reflectance of snow is at around 500 nm, but at this wavelength the penetration of the signal into the snowpack reaches about 0.1 m (Deems et al., 2013), so the reflected signal does not represent only the snow surface. The optimal wavelengths are at 900-1100 nm, where the reflectance of snow is high, and the majority of the signal is reflected from the top 0.01 m (Deems et al., 2013). A lidar sensor especially developed for the application to snow and ice is the Riegl VZ6000 terrestrial laser scanner (TLS). It uses a wavelength of 1064 nm and has a measurement range of up to 6000 m. It is used in various applications, often to measure glaciers at large scale (Voordendag et al., 2021; LeWinter et al., 2014), or studies to monitor snow surface variations and avalanche properties (Hancock et al., 2018a, b; Fey et al., 2019; Hancock et al., 2020). However, the Riegl VZ6000 TLS is very costly, it operates in laser class 3B and is not eye-safe in its optimal operation mode at short ranges (few hundred meters). Autonomous operation is very challenging during winter in an alpine environment, because of the required power supply, stable setup of the sensor, and weather protection (Voordendag et al., 2023).

Alternatives can be found in the automotive industry, where the market for low-cost lidar sensors is evolving fast. Many of these sensors have a wavelength of around 900 nm, are mechanically and environmentally robust, designed for year-round outdoor use, and operate in the short to medium range (maximum few hundred metres). Snow scientists have already used such sensors to measure snow cover properties either using UAVs (Jacobs et al., 2021; Dharmadasa et al., 2022; Koutantou et al., 2022), or ground-based mobile platforms (Jaakkola et al., 2014; Donager et al., 2021; Goelles et al., 2022; Kapper et al., 2023).

Herein we present a monitoring system, that uses a low-cost lidar sensor in a static ground-based setting with automatic and autonomous operation. The aim is to monitor the snow depth variations in an avalanche release area at high spatiotemporal resolution. In this paper we describe the monitoring system and the experiences from the first operating season. We also present preliminary results and case studies, that show the potential and limitations of the proposed system.

2 Monitoring system

The purpose of the monitoring system is to build up a snow depth database of high spatial and temporal resolution covering an avalanche release area. The main snow depth measurements are done using lidar sensors. RGB images collected using single-lens reflex (SLR) cameras complement these data. Additionally, we installed meteorological sensors at the stations to observe wind speed and direction, air temperature, relative humidity, and snow surface temperature. These data will later serve as input data for a modelling approach, where we aim to predict the snow depth variations. The system is ground-based, operates autonomously (power supply by solar panel and wind turbine) and transfers the data regularly to a server (once per hour) which
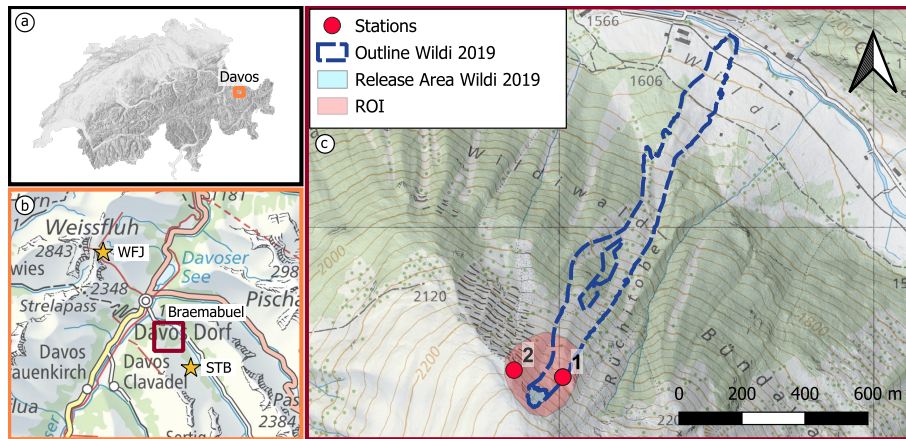
Figure 1. Overview of the study area with (a) the location of Davos in Switzerland, (b) the location of Braemabuel in the area of Davos and the locations of nearby weather stations Weissfluhjoch (WFJ) and Stillberg (STB), and (c) a close up map of the study area Braemabuel, with the outline and release area of the Wildi avalanche in 2019, the region of interest (ROI) around the typical release area, and the location of the measurement stations Braema1 (1) and Braema2 (2) (map source: Federal Office of Topography).

allows for remote monitoring and data analysis. In the remainder of this section, we elaborate on the study site and setup, the chosen instruments, power supply and communication, and the photogrammetric data which we used for validation.

2.1 Study site and setup

The study site is the release area of the "Wildi" avalanche path at Braemabuel, in the Dischma valley, a high-alpine valley in the area of Davos in southeast Switzerland (Fig. 1). The valley is permanently inhabited, and the road is kept open in winter. Several avalanche paths threaten the road, and it had to be temporarily closed several times in the past years due to avalanche danger (Zweifel et al., 2019). The slope of the study site faces northeast and has an inclination of 30–45 degrees. Figure 1 shows an overview of the study site with the mapped outlines of the Wildi avalanche from 2019, as an example of a recent large avalanche in this area. For a suitable coverage of the region of interest we installed two stations. Their locations were determined in three steps: 1) checking the geometrically possible maximum view-shed for the laser beam in a GIS tool, 2) checking the typical snow depths using previous snow depth acquisitions of the area to ensure that the station would not get buried, 3) checking the surroundings of possible locations on-site, in the field to find suitable mounting possibilities, such as stable bedrock.

Station Braema1 (Fig. 2a) is mounted on the side of a large rock in the middle of the slope, on a subtle ridge at an altitude of 2191 m a.s.l., where the the snow depths are shallower than the average of the area, as the snow tends to be eroded by the wind, at this location. Station Braema2 (Fig. 2b) is located on the top of the main ridge (altitude: 2255 m a.s.l.), just high enough to get more sunlight, but low enough to be able to view into the region of interest. The pole carrying all equipment is screwed directly to the rock on the ground, at this location. Both stations were installed on 23 November 2023.
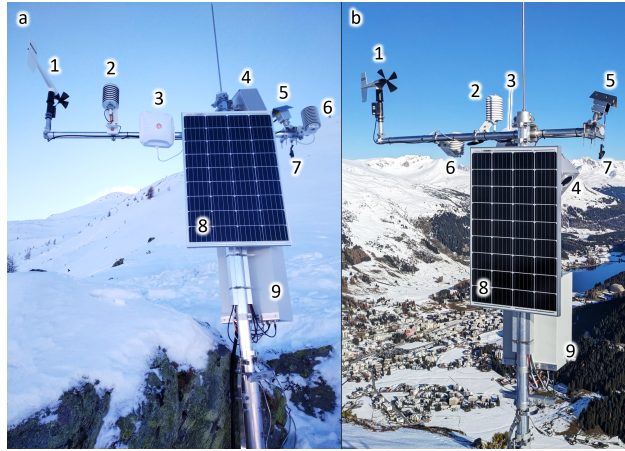
Figure 2. Station Braema1 (a) and Braema2 (b) with 1) anemometer (wind speed and direction), 2) HygroVUE10 (air temperature and relative humidity), 3) communication antenna, 4) camera system, 5) Livox Avia, 6) SnowSurf (snow surface temperature), 7) prism, 8) solar panel, 9) control box (photo: Pia Ruttner).

In order to register the lidar point clouds between epochs, identifiable stable areas or targets in each scan are required. For this purpose, we mounted several mini-prisms in the region of interest, choosing places that are assumed to be stable and that are not completely covered in snow in the winter season (Fig. 3). However, there were no suitable locations for a geometrically ideal distribution of the prisms (surrounding the ROI such that no extrapolation is needed within the georeferencing), and no locations on the slope to be visible from the upper station (Braema2). Looking from top, the terrain will be snow covered during the winter season. Therefore, we configured the viewing angle of the upper lidar sensor such that its point cloud has a maximum possible overlap with the point cloud from the lower sensor (Braema1). This gives the possibility to register the scans within each epoch directly using the point clouds from the two stations, and register them between the epochs by georeferencing using the prisms.

For the purpose of relating the point clouds or the derived results, such as digital surface models (DSMs), to a superordinate coordinate system (e.g., the Swiss national system LV95), we measured the prism centers using a Leica TCR1203 total station and connected these measurements to a local network of benchmarks, which we measured using a Trimble real-time kinematic (RTK) Global Navigation Satellite System (GNSS) unit.

2.2 Instrumentation

2.2.1 Lidar

The most important criteria for the lidar sensor in our application are the operating wavelength, maximum range, suitability for outdoor use, and cost. In the fast evolving market of low-cost lidar sensors, most of the devices are now solid-state sensors operating with 32, 64 or 128 scan lines (Altuntas, 2022). In a mobile application, the scan lines sweep across the scene as the
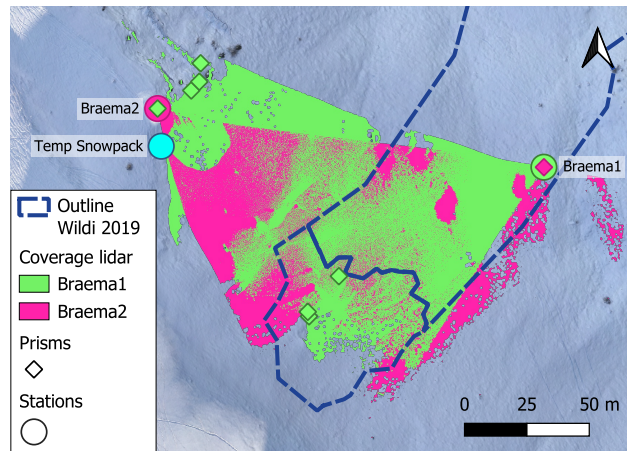
Figure 3. Map of the study area, with the spatial coverage of the two lidar sensors, the measurement stations (including the station to measure temperatures within the snowpack "Temp Snowpack") and the prism locations. The color of the prisms indicates which prism is visible from which station. The coverage of the stations is derived from the acquisition of 23 December 2023. The background image is derived from UAV data from 19 December 2023.

sensor itself moves, thereby increasing the spatial coverage. In a static setup the fixed angular spacing between the scan lines of solid-state sensors results in relatively sparse coverage of the scanned scene, especially at far ranges.

Based on a market survey of lidar sensors and their technical specifications, we selected the Livox Avia lidar sensor for our measurement system. This sensor uses a Risley prism-based non-repetitive scanning pattern (Vuthea and Toshiyoshi, 2018) instead of fixed scan lines. This allows for a successively denser spatial coverage with increasing scanning times, also when not moving the sensor itself (Fig. 4). Furthermore, the selected sensor operates at a wavelength of 905 nm, has laser class 1 (i.e., it is eye-safe), has a maximum detection range of 450 m, a low power consumption of 8 W and costs around 1.5k USD. Further specifications, compared to similar lidar sensors on the market, are listed in Table 1.

2.2.2 Camera

A camera provides visual information about the conditions and processes in the release area, such as weather conditions, or traces of avalanche events, animals and sportspersons. We chose a Canon EOS R7 32 megapixel camera with an RF-S 18-45 mm F4.5-6.3 IS STM zoom lens. This setup allows an on-site adjustment for capturing roughly the same area with the camera as for the lidar sensor. The camera operates in aperture-value (Av) mode, with the aperture set to f/8. The shutter speed is automatically adjusted by the camera for optimal exposure. This allows for acquisitions at day and—during periods with sufficiently strong moon light—at night (Fig. 5).

0.1 s	0.5 s
1 s	3 s
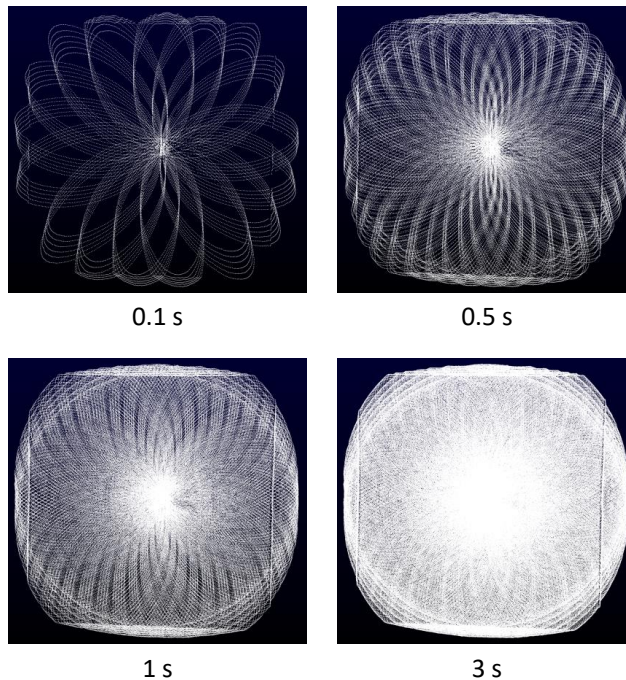
Figure 4. Scanning pattern of the Livox Avia lidar sensor in an indoor test setting. We display the scanning pattern for 0.1, 0.5, 1.0 and 3.0 seconds scanning time (the flattening on top and bottom, and the linear features on the sides are related to the shape of the scanned room).

Table 1. Specifications of selected lidar sensors. Values that are not published by the manufacturer are denoted with "-". The classes for the approximate costs are: low <10k USD, medium 10-25k USD, high >= 100k USD.

Specification	Livox Avia	Hesai Pandar128	Ouster OS2	Quanenergy M8-Prime Ultra	Velodyne Alpha Prime	Riegl VZ6000
Wavelength [nm]	905	905	865	905	903	1064
Max. range [m]	450	200	350	200	245	6000
Field of View (HxV)	70.4° x 77.2°	360° x 40°	360° x 22.5°	360° x 20°	360° x 40°	360° x 60°
Range Accuracy	-	2-10 cm (1-200 m)	5 cm	3 cm (1σ @ 50m)	3 cm	15 mm
Range Precision	2 cm (1σ @ 20m)	-	2-10 cm	-	-	10 mm
Angular Precision (1σ)	<0.05°	-	0.01°	-	-	0.0005°
Beam Divergence	0.28° × 0.03° (VxH)	-	0.09° (FWHM)	-	-	0.007°
Laser Class	1	1	1	1	1	3B
Power Consumption [W]	8	23-27	18-24	19	22	75
Cost	low	medium	medium	medium	high	high

Figure 5. Example images of camera at station Braema1 (see Fig. 1) on 31 January 2024, at midnight (00:00 UTC) and in the morning (08:00 UTC). The distance to station Braema2 on the ridge is about 160 m.

2.2.3 Meteorological sensors

We also installed various meteorological sensors. We record the wind speed and direction using a Young Wind Monitor 05103-L, the relative humidity and air temperature using a Campbell HygroVUE10, and the temperature of the snow surface using a Waljag SnowSurfSDI sensor. Additionally, we measure the temperature in the snowpack, in the vicinity of station Braema2 , at the same height and exposition as the avalanche release area (see Fig. 3). To do this we installed three poles with different heights (0.4, 0.6 and 0.8 m above ground) next to each other, each equipped with a GeoPrecision M-Log 5W temperature sensor on top. We do not use these data in the present investigation, but nevertheless list them here to complete the information on the equipment of the test site.

2.2.4 Power and communication

The measurement stations are designed to operate autonomously. Therefore, they are equipped with a solar panel (115 Watts), and station Braema1 additionally with a wind generator (Phaesun Stormy Wings 400W) for times when the station does not get enough sunlight. The data collected on-site are regularly transmitted to a server so they can be analysed in (near) real-time. This makes it possible to recognise malfunctions at an early stage. The remote connection and control are particularly important, as it can be dangerous to access the measurement stations during the winter months due to occasional high avalanche danger.

2.3 Configuration and data processing

2.3.1 Measurement configuration

Figure 6 shows a schematic view of all sensors and connections. The measurement system is configured, such that it uses a minimal amount of energy. This means that most instruments and sensors are turned off most of the time, except for the meteorological sensors which need very little energy, and the datalogger, which controls all measurements and data transfers. The data from the meteorological sensors are captured and locally stored by the datalogger every 30 min. At a specified time
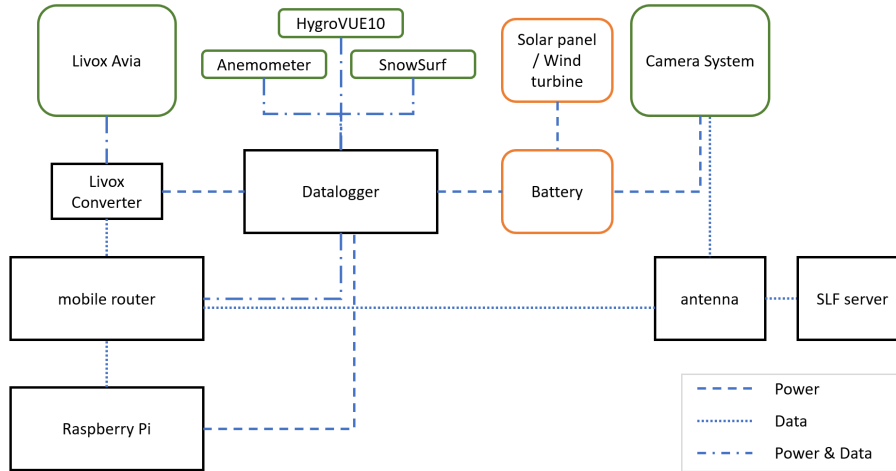
Figure 6. Schematic view of all sensors and connections. Sensors are in green boxes, power-related components are in orange boxes and all communication modules are in black boxes. Dashed lines indicate power connections, dotted lines data communication and the combination of both, indicates a combined connection (power and data).

interval (once per hour) the datalogger supplies a Raspberry Pi computer, a mobile router and the Livox Converter with power for 15 min. As soon as the Rasperry Pi is powered on, it tries to establish a connection with the lidar sensor through the mobile router and the Livox Converter. In case of successful communication, the Raspberry Pi triggers a lidar scan which takes 5 s. The scan data are then stored on the local solid-state drive (SSD) of the Raspberry Pi. If the Raspberry Pi is not able to connect with the Livox Avia sensor within 120 s, it sends an error message to the technical support. After a successful scan the Raspberry Pi sets the Livox sensor to power-saving mode, and transfers the data from the local SSD to a remote server via mobile router and 5G antenna. During the time the router is switched on, the server also retrieves the meteorological measurement data from the logger. The operation of the camera works independently. The photos are triggered at the same time as the lidar scans and are immediately transmitted to the remote server through the 5G antenna.

2.3.2 Data processing

The point clouds of the Livox Avia sensors are first converted from the sensor's binary LVX format to the standard LAS format using a Python script. Afterwards, the point cloud from station Braema2 is transformed to the local scanner's own coordinate system of the point cloud from station Braema1 using the Open3D data processing library (Zhou et al., 2018) implementation of the Iterative Closest Point (ICP) plane-to-plane algorithm (Besl and McKay, 1992; Chen and Medioni, 1992). In order to register the different scan epochs with each other, and reference them to a global coordinate system, we use the prisms, which are installed in the area of interest (see Fig. 3). To determine the prism center coordinates in the local scans we filter the points in the scan that belong to the prism and perform a 2D-Gaussian fit using the intensity values (Schmid et al., 2024). With the
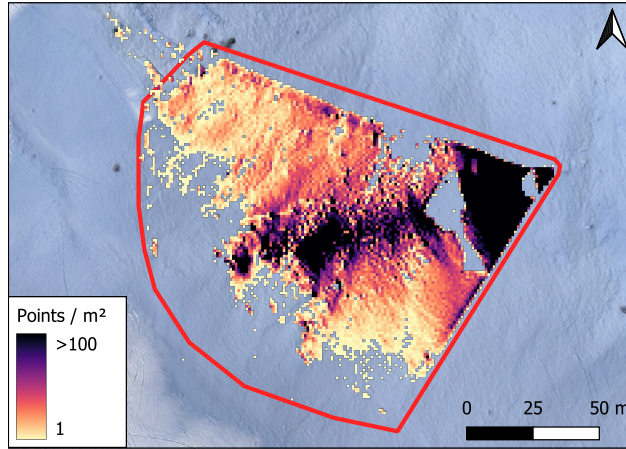
Figure 7. Point cloud from station Braema1 (24 November 2023, 12:00 UTC) on a 1 m grid, with a customized region of interest (red polygon). The grid cells are colored by their point density. The background image is derived from UAV data from 19 December 2023.

known global coordinates of the the prism centers (see Sect. 2.1), we compute the transformation matrix from the local to the global coordinate system.

For the computation of snow depth changes we create a gridded DSM per epoch, using the open source software Cloud-Compare, and calculate the difference between the DSMs. In particular, we perform the following steps: We define a grid with a cell size of $0.1 \times 0.1 \, \text{m}$, which is the average resolution of the point cloud. The elevation value assigned to each cell is the average elevation value of all points that fall within that cell. Empty cells are filled with the linearly interpolated height value from the nearest neighbouring cells that are not empty. This is based on Delaunay triangulation, where we define the maximum edge length as 1 m. Empty cells beyond the maximum edge length are filled with the empty cell value "-999". For the analysis of the temporal variations of the spatial coverage of our ROI we define a horizontal $1 \times 1 \, \text{m}$ grid, counting each grid cell as covered if there is at least one scan point whose horizontal coordinates are within that cell. We then quantify the coverage as percentage of the grid (ROI, red outline in Fig. 7, approx 14'500 m^2) that was covered by the lidar.

2.4 Photogrammetric UAV data for validation

We acquired a reference dataset using a Wingtra One Gen II fixed-wing UAV with a Sony DSC-RX1RM2 42 megapixel camera. The UAV is equipped with an onboard high-precision global navigation satellite system (GNSS) receiver which records the position of each captured image. We used data from a reference station nearby (3 km distance to the measurement site), operated by the Swiss Positioning Service (swipos), to compute the coordinates in the Swiss national coordinate system LV95/LN02, using post-processing kinematcs (PPK). For further photogrammetric processing we used the software Agisoft Metashape Professional, Version 1.6.5. The photogrammetric workflow, using structure from motion (Koenderink and Doorn, 1991), is described in previous publications (Bühler et al., 2016; Adams et al., 2018; Eberhard et al., 2021) and the software manual (Agisoft, 2020). For the accuracy assessment of the photogrammetric model, we used checkpoints during the acquisition,

which are square black and white checkerboard targets, with a side length of 0.4 m. We measured the center of the targets with a Trimble RTK GNSS unit. The targets are visible in the photogrammetric model as well and can be used as independent check points. This means that the targets are not used in the photogrammetric processing but serve to validate the accuracy of the model. The resulting photogrammetric model has a horizontal resolution of 0.1 m. The area covered by the UAV is 1.4 km^2 and includes the entire area covered by the lidar. By subtracting a snow-free DSM, acquired in autumn with the same drone and sensor, we generate a spatially continuous snow depth map.

In order to compare the lidar scans with the photogrammetric model, both datasets need to be in the same coordinate system. Therefore, we transform the local lidar scans to the superordinate coordinate system (LV95/LN02), using the prisms in the study area, as described in Sect. 2.3.2. Due to the unfavourable geometric distribution of the prism locations, we use this approach for a coarse alignment, and the ICP algorithm for the fine registration.

3 Results

In this section we present preliminary results derived from the data acquired during the first season of operation, i.e., until 14 April 2024. On this day a large glide-snow avalanche destroyed station Braema1. We have investigated the relation between the meteorological parameters and the lidar coverage of the region of interest (Sect. 3.1), carried out a first comparison of the snow surface obtained from our system and a photogrammetry-derived surface from a UAV (Sect. 3.2), and performed two case studies showing an avalanche event and a snowfall event, respectively (Sect. 3.4).

3.1 Lidar spatial coverage of region of interest

The maximum spatial coverage of the area of interest depends on the sensor specifications (e.g., the measurement range), the number, spatial distribution and orientation of the lidar sensors, the angle-of-incidence of the laser beams, shadowing effects due to the topography, the weather situation, and the snow surface conditions. As an example, Fig. 3 shows the spatial coverage at our study site (including both stations) on 23 December 2023, 16:00 UTC. However, changes over time are to be expected. We analyze this in detail for station Braema1. Figure 8b shows the spatial coverage of station Braema1 over time, together with relevant meteorological parameters, namely incoming short-wave radiation (ISWR), snow surface temperature (TSS), height of new snow (HN) within 24 hours, and relative humidity (RH). The ISWR data (Fig. 8a, color) are from the nearby weather station Stillberg (STB), about 2 km away from Braema1 and with a similar exposition and elevation (see Fig. 1). The TSS observations are from the instrument at station Braema1 (Fig. 8a, line). The amount of new snow HN (Fig. 8c, color) is taken from the nearby weather station Weissfluhjoch (WFJ), about 5.5 km away from Braema1, but at similar elevation (see Fig. 1). In this context we use the value of HN as an indicator if there was a snowfall event, and how intense it was. The relative humidity is measured directly at Braema1 (Fig. 8c, line).

The maximum spatial coverage of the ROI obtained from Braema1 is about 70% (Fig. 8b), as the surfaces more than 120–150 m away from the station are hardly covered by the lidar sensor (Fig. 7). This uncovered area is however mostly covered by Braema2 (see Fig. 3). The spatial coverage decreases during snowfall events and with high relative humidity. It can be as low

230 as 0%. Even if HN indicates accumulation of new snow, this does not mean that it has been snowing continuously during the preceding 24 hours. Due to the high temporal resolution of the lidar system, a short weather window during a snowstorm will allow the system to capture the area and provide current information about the snowpack.

There are three periods with big data gaps, one in mid-December 2023, one at the beginning of January 2024 and one at the beginning of April 2024 (Fig. 8b, light yellow areas). A review of the camera images shows, that the camera's lens was
235 covered by snow on these dates. We conclude that most likely, also the front side of the lidar sensor was covered by snow, and the sensor could therefore not scan the area of interest. However, the coverage increases again as soon as the humidity drops. We assume that the drop of humidity indicates the end of the precipitation and that this coincides with the clearing of the lidar lens.

A comparison of the spatial coverage with the ISWR, especially during periods without precipitation, shows a clear diurnal
240 pattern. Around the time of the winter solstice there is no direct sunlight in the ROI at any time of the day, and there is no significant difference between coverage at day and at night (e.g. the period after 15 December 2023). With the beginning of the year, the ISWR in the ROI increases, and a diurnal pattern of changing spatial coverage with better coverage during the nights becomes apparent. The difference of spatial coverage between day and night reaches up to 30 % in mid March. Later in the season, the spatial coverage decreases also during nighttime, when the TSS is at or gets close to 0°C.
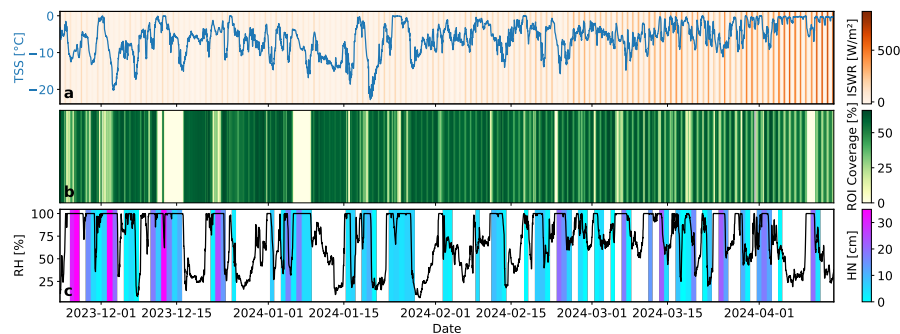
Figure 8. a) Incoming short wave radiation (ISWR, color) and snow surface temperature (TSS, line), b) spatial coverage of the ROI (color), and c) new snow height (HN, color, white indicates no new snow) and relative humidity (RH, line).

245 **3.2 Comparison with photogrammetric data**

Figure 9 shows the vertical differences between the DSMs, which are derived from a UAV photogrammetric acquisition and the lidar point clouds on 19 December 2023, 11:00 UTC. The difference of the two DSMs has a mean of 0.005 m and a standard deviation of 0.15 m. The differences of the DSMs are larger and noisier at the respective far ends of the lidar data. There are also some artifacts which are due to the raw processing status of the lidar point cloud. For example, at the border of geometrically
250 occluded areas where the angles of incidence are large and the point clouds likely contain mixed pixels (points that are in

erroneous locations due to the comparably large lidar footprint and the impact of signal back-scattering by objects/surfaces at different distance).

Figure 10 shows the relative differences in snow depth between 19 December 2023 and 6 February 2024 from two lidar point clouds (Fig. 10a) and, analogously, from two photogrammetric UAV acquisitions (Fig. 10b). The observed snow depth changes from the lidar point clouds range between -1.2 and 0.8 m, which is similar to the ones obtained from the photogrammetric data with a range between -1.3 and 1.0 m. The biggest disagreement between the acquisition methods is again visible towards the edges of the lidar swath at areas far away from the sensor (Fig. 10c). Overall, the results differ by a mean of 0.03 m, and the standard deviation of the differences between the UAV results and the lidar results is 0.19 m, see Fig. 10c.

3.3 Uncertainty assessment

The accuracy of the photogrammetric model is evaluated with the use of check points. The GNSS-based coordinates of the check point centers have an accuracy of 0.01 m horizontally and 0.02 m vertically. The distances between the measured (GNSS) and the estimated (photogrammetric model) positions of the check point centers are 0.03 m and 0.02 m, horizontally and vertically. The accuracy of the photogrammetrically derived snow depths are not explicitly examined in this study, but from literature we assume a vertical accuracy of around 0.1 m (Nolan et al., 2015; Vander Jagt et al., 2015).

The uncertainty assessment of the lidar data needs further research and investigations. Here we give an overview of the most common error sources (Schaer et al., 2007; Voordendag et al., 2023), and a rough estimation of the expected magnitudes:

- Registration: The intra-epoch-alignment of the pointclouds of both scanners is done with ICP, where the root mean square error (RMSE) of corresponding inliers is on the order of 0.05-0.1 m.

- Scanning geometry: The beam divergence and incidence angle define the size of the footprint of the laser beam on the reflecting surface. With a beam divergence of 0.03° (horizontal) x 0.28° (vertical) the footprint measures 0.05 m x 0.5 m on a target at 100 m distance, perpendicular to the scanning direction (incidence angle of 0°). In our study area the incidence angles are between 30° and 85°. For example, following the methods in Voordendag et al. (2023) and Schaer et al. (2007), a point at 50 m distance from our sensor, with an incidence angle of 50°, in an area of 30° slope gradient, results in a vertical uncertainty of 0.06 m. However, this value strongly depends on the distance from the station, the incidence angle and the local slope gradient. With a more unfavourable geometry (100 m distance, 70° incidence angle, 35° slope gradient), the vertical uncertainty gets as big as 0.3 m.

- Atmospheric conditions: Measurement errors due to changing atmospheric conditions are on the level of a few millimeters at short measurement ranges (100 m) and can therefore be neglected in our application.

Further important limitations are given by the hardware, the surface reflectivity of the snow (in particular with free water present) and the final combination of all mentioned uncertainties. With the steadily growing dataset from our stations we plan to further investigate these uncertainties. With the current knowledge and the comparison to the photogrammetric data, we assume the lidar data to have an uncertainty in the range of 0.1-0.3 m.
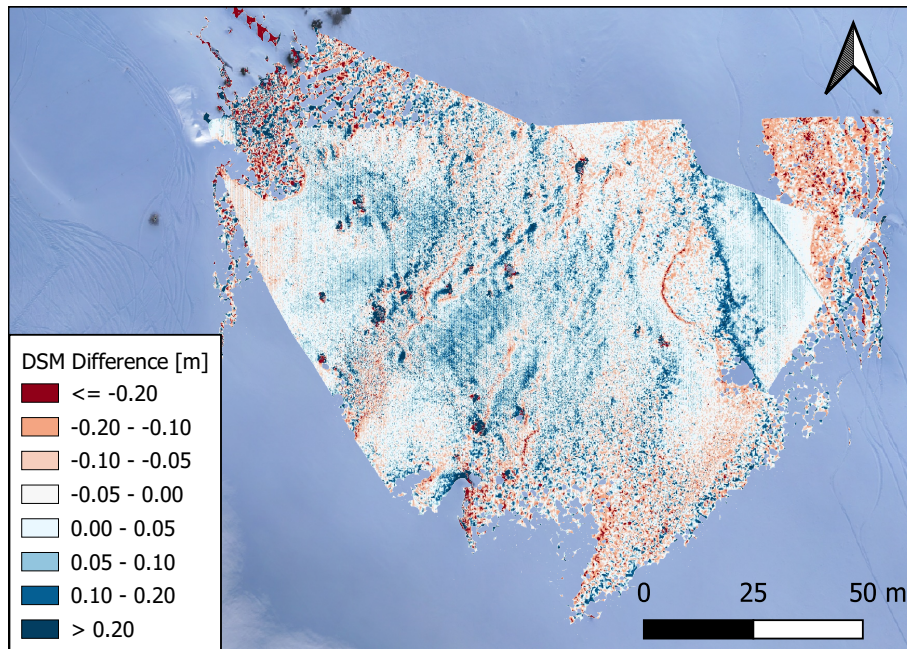
Figure 9. Difference of the DSMs from a UAV photogrammetric acquisition and the lidar point clouds on 19 December 2023, 11:00 UTC. The background image is derived from the UAV data. Ski and snowboard tracks are visible outside of as well as cutting through the monitored area.
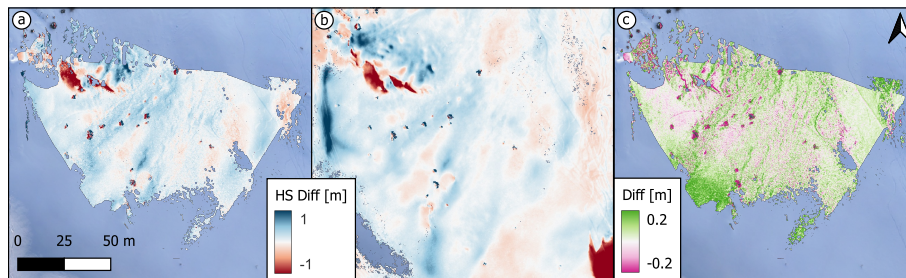
Figure 10. Comparison of the snow depth (HS) differences between 19 December 2023 and 6 February 2024, from a) the lidar point clouds and b) photogrammetric UAV acquisitions. The discrepancies between a) and b) are shown in c). The background image is derived from UAV data from 19 December 2023.

3.4 Case study I: Avalanche event

On 10 December 2023 a small avalanche occurred in the ROI. Figure 11 shows the snow depth changes from before to after this avalanche event. Dark red areas indicate snow erosion and blue areas indicate snow deposition. The release area, crown (fracture line), and track of the avalanche are well visible and the areas not affected by the avalanche do not show big differences between the consecutive epochs.
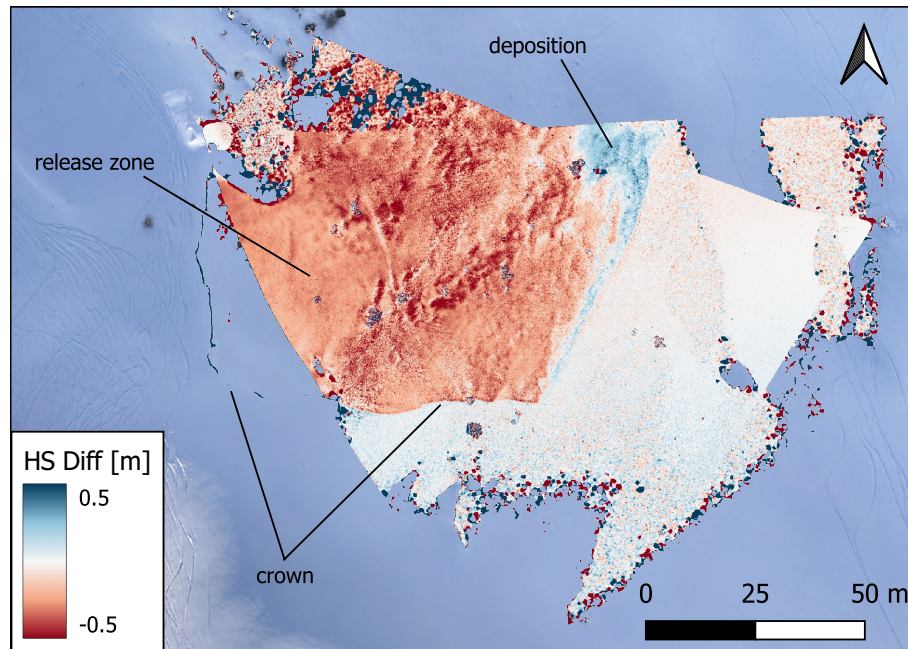
Figure 11. Snow depth (HS) differences derived from lidar acquisitions on 10 December 2023 at 11:00 and 12:00 UTC, showing an avalanche event in the ROI. The background image is derived from UAV data from 19 December 2023.

The crown has a height of approximately 0.2 m and the eroded area has a width and a length of 100 m, though, the length of the eroded area can only be approximated, since the avalanche path extends outside of the monitored area. The upper part of the release area is not covered by Braema2, due to its limited field of view, and scarcely by Braema1, due to its range limitation with the high incidence angles in that area. The influence of the incidence angle on the range limitation is demonstrated by the appearance of the crown in the second epoch. There were no points recorded in that area before the avalanche, but with the decreased incidence angle on the crown we can observe it in the second epoch. This captured avalanche data, combined with the meteorological observations, will become useful input data in future avalanche modeling of the Wildi avalanche path.

3.5 Case study II: Snowfall event with wind

Strong winds accompanied by snowfall were observed in the ROI between 22 and 23 December 2023. Figure 12 shows the meteorological conditions around this period, including the wind speed and direction from station Braema2 (30 min average values in blue, and the maximum gusts in orange), and the 24 hour new snow amount from the measurement station at Weissfluhjoch. On 22 December 2023, the wind was coming from the west, with an average speed around 25 km h^{-1}, and gusts up to 80 km h^{-1}. On that day, there was 0.25 m of new snow recorded at Weissfluhjoch. The influence of the strong west wind is clearly visible in the redistribution in the snow depth from 21 and 23 December 2023 (Fig. 13). The snow redistribution was influenced by small terrain features within the ROI, such as erosion on taller small sub-ridges and deposition in lee-ward
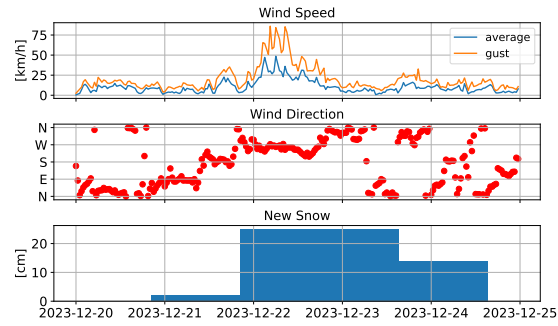
Figure 12. Meteorological conditions (wind speed and direction and amount of new snow) in the ROI in the period of 20-25 December 2023.
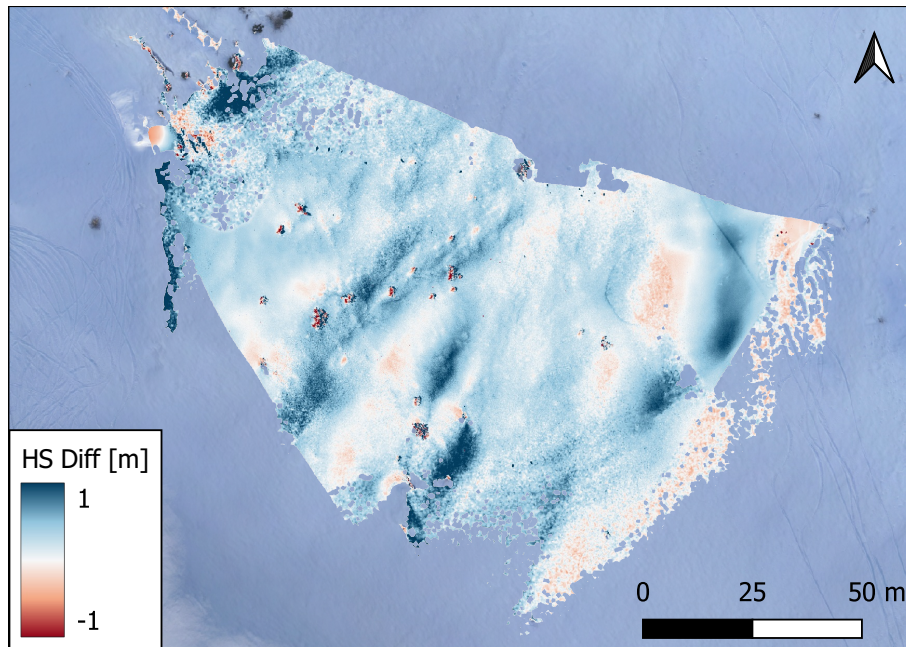
Figure 13. Snow depth (HS) differences derived from lidar acquisitions on 21 December 2023, 07:00 UTC and 23 December 2023, 16:00 UTC.

depressions and small gullies. This snow redistribution is also visible in the snow depth changes from the lidar data and agree with the recorded mainly westward wind direction on this day.

4 Discussion

Here we will discuss the potential and limitations of the system, looking at the aspect of meteorological influences on the possible coverage of the region of interest, the comparison of the lidar data with a photogrammetrically derived model and its applicability and practical implications.

4.1 Meteorological influences on region of interest coverage

Some meteorological conditions, e.g. fog and precipitation, can hamper lidar acquisitions, resulting in a reduction of lidar transmission and reflectance. One factor of the received intensity of signals at the surface is the solar radiation. With the presence of ambient radiation in the same range of wavelength as the sensor emits, the signal to noise ratio decreases, which leads to missing weak signals, e.g. at far ranges from the sensor or at low incidence angles on the measured surface (Prokop, 2008). Another factor is the presence of liquid water, which can be derived from the TSS being close to or above 0°C. Since the spectral refractive index of water and ice are very close, the main effect of decreased returned intensity is the increase of snow grain sizes, which leads to increased absorption and spectral reflection (Wiscombe and Warren, 1980; Warren, 1982; Prokop, 2008). Precipitation and fog strongly limit the possible field of view. Depending on the intensity of snowfall, we are still able to measure up to about 100 m during light snowfall, but the view can also get limited to only a few meters during strong snowfall. The high temporal resolution in our setup enables acquisitions in short weather windows, which offers a valuable alternative for when other methods (e.g. UAV flights) would not be feasible.

4.2 Comparison of lidar data and a photogrammetric model

While there are discrepancies between the photogrammetic UAV-based acquisitions and the early processing results from our lidar system, we consider the agreement between the photogrammetric data and our lidar acquisitions an indication that the lidar-based system is able to provide snow depth differences with high spatial and temporal coverage. The comparison with the phtogrammetric model shows the largest uncertainties at the far ranges from the lidar sensors and where the pattern changes from ablation to accumulation. Although we performed a horizontal alignment between the models, there remain unavoidable imperfections, which result in deviations most visible in the mentioned areas. Due to the ground-based setup the accuracy of the lidar measurements strongly varies across the slope with varying distances of the measured points from the sensor and varying angles of incidence. With airborne acquisitions, it is possible to keep the sensor at a (roughly) constant distance above ground and achieve more favorable angles of incidence over the whole measurement area. This implies less variation in measurement uncertainty due to more constant measurement configuration.

The quantification of the currently achieved and achievable accuracy will need further investigations and dedicated experiments, including an extended assessment of the quality of the photogrammetrically derived snow depths from the UAV as well as an improved co-registration of UAV and lidar products, and the impacts of large angle-of-incidence and mixed pixels in the lidar data.

4.3 System applicability and practical implications

In comparison with current state-of-the-art methods our system design has a few advantages. The ground-based, autonomous measurements allow for higher temporal resolution than airborne approaches (Bühler et al., 2016; Bührle et al., 2023; Jacobs et al., 2021). The use of lidar technology enables acquisitions with high spatial resolution at day and night, opposed to purely photogrammetric methods that are limited by daylight (Basnet et al., 2016; Filhol et al., 2019). Ground-based, autonomously operating lidar sensors have been installed before, but at significantly higher costs and effort, in terms of sensor protection, stability and power supply (Voordendag et al., 2021). When selecting the sensors for our system, we therefore explicitly focused on outdoor suitability, low power consumption, and low cost.

However, finding a suitable location for installation of the system might be challenging in some areas. There needs to be a suitable setup possibility (e.g. large rocks, stable ground), at locations where the geometrically possible view of the system can cover the desired area of interest. There is always a compromise in possible ROI coverage, and risk exposure when setting up a station in, or close to an avalanche release zone. For a meaningful comparison between epochs, and with data from other platforms, identifiable and stable targets are needed in the ROI. Though, these are not always naturally available and suitable locations where artificial targets can be installed may be limited. However, the system itself is designed in such a way that the configuration can be easily adopted. Because it runs autonomously, it can be used in areas that would be too dangerous to carry out manual snow sampling campaigns and due to it is low-cost, multiple systems can be installed and used simultaneously.

The two presented case studies show the potential and some limitations of the proposed system. We can detect small-scale snow depth variations and also an avalanche is clearly visible in the data. The high temporal resolution of the lidar system enables us to capture an avalanche event by measuring the snowpack surface shortly before and after an event. This allows the estimation of release depth and volume from the measurements. With the limitation of the maximum possible range of the lidar system, we are not able to cover the full slope, or whole avalanche tracks. However, we can capture small release areas, or parts of larger ones. This may help to assess the conditions in a release area, determine local snow drift patterns, and in case of an avalanche, at what depth the weak layer was. Jointly, this is important information for avalanche formation research and simulations.

5 Conclusions and outlook

Wind-drifted snow can strongly influence slope stability, but local and up-to-date information is rarely available. Therefore, we developed a low-cost monitoring system to deliver near real-time data of the snow depth variations in avalanche release areas. The monitoring system presented herein autonomously captures snow depth variations at high spatial (cm to low decimeter) and temporal (hourly) resolution. We designed two stations, that are installed in an avalanche release area close to Davos in Switzerland. They were in operation from November 2023 through April 2024.

The analysis of the relative changes of spatial coverage of the region of interest provides an initial indication of the influence of the snow surface and weather conditions on the measurement performance. A comparison of snow surface models derived from lidar and photogrammetric UAV data shows a mean height difference of 0.005 m with a standard deviation of 0.15 m,

indicating an accuracy of the lidar data at a low decimeter level. We achieve a similar agreement between the two systems (lidar and photogrammetric UAV data) when comparing snow depth changes between acquisitions from 19 December 2023 and 6 February 2024. On 10 December 2023 an avalanche event occurred in the study area, which was well captured by the system, allowing estimates of the width of the release area (about 100 m), as well as the average release height (about 0.2 m). In a second case study, we were able to demonstrate the potential for investigating wind-induced snow depth redistribution during a 3-day snowfall event with strong winds.

The first season of system operation also revealed some limitations and areas of opportunity for improvement. Limitations include the maximum possible range of the sensor and achievable accuracies. This is due to the sensor specifications, but also unfavourable scanning geometries due to the setup configuration. The latter, i.e. ground-based installation in the same slope as the monitored area, also causes unavoidable shadowing effects in the acquired data. We see room for improvement in further processing of the data, including automated procedures for data filtering, smoothing and georeferencing. Future investigations will also include additional comparisons with other sensors (e.g. the Riegl VZ6000 laser scanner and and DJI L2 lidar UAV) and dedicated experiments (e.g. the effect of light on the sensors) in order to better quantify the performance of the monitoring system.

The newly established database will be expanded in the following seasons, including data from additional sensor installations at a nearby avalanche release area with different exposition and at the Nordkette close to Innsbruck, in collaboration with the Austrian Research Centre for Forests BFW. We will compare the nearby weather stations in Davos with long data records, currently applied as the main information source for decision making during avalanche periods, to the snow distribution dynamics within the monitored avalanche release zones. Furthermore, we will use the high spatiotemporal resolution data of snow depth changes, together with the recorded meteorological parameters for the refinement of avalanche simulations, as well as for the validation of existing and the development of new small-scale wind-drifting snow models. Such models can for example be applied to better inform large scale avalanche hazard indication modeling (Bühler et al., 2022; Issler et al., 2023) where the assumptions on the impact of wind-drifted snow on avalanche release depths are still very basic.

In the future, we plan to make the measurements from the release zones available to the local hazard experts by a digital information platform to support their decisions on temporary avalanche mitigation and safety measures.

Code and data availability. The data and codes applied will be available on ENVIDAT (https://envidat.ch) upon the acceptance of this paper.

Author contributions. Study design: YB, PRJ and JG, Technical implementation: TH, Fieldwork: PRJ, JG, and TH, Data processing: PRJ, with inputs from AV, AW and YB, Manuscript: PRJ with contributions from all co-authors.

Competing interests. One of the (co-)authors is a member of the editorial board of Natural Hazards and Earth System Sciences.

Acknowledgements. This research is funded by the Swiss National Science Foundation SNSF with the project "Avalanche Safety for Roads" (Nr. 207519). We thank the SLF workshop for designing and producing the hardware for the measurement stations, Andreas Stoffel for operating the Wingtra UAV and Jor Fergus Dal and Justine Sommerlatt for their support during field work. We thank the reviewers Katreen Wikstrom Jones and Alexander Prokop, and the editor HP Marshall for their valuable feedback, which significantly improved the manuscript.

References

Adams, M. S., Bühler, Y., and Fromm, R.: Multitemporal Accuracy and Precision Assessment of Unmanned Aerial System Photogrammetry for Slope-Scale Snow Depth Maps in Alpine Terrain, Pure and Applied Geophysics, 175, 3303–3324, https://doi.org/10.1007/s00024-017-1748-y, 2018.

Agisoft, L.: Agisoft Metashape User Manual - Professional Edition, Version 1.6, https://www.agisoft.com/pdf/metashape-pro_1_6_en.pdf, 2020.

Altuntas, C.: Point Cloud Acquisition Techniques by Using Scanning Lidar for 3d Modelling and Mobile Measurement, The International Archives of Photogrammetry, Remote Sensing and Spatial Information Sciences, XLIII-B2-2022, 967–972, https://doi.org/10.5194/isprs-archives-XLIII-B2-2022-967-2022, 2022.

Basnet, K., Muste, M., Constantinescu, G., Ho, H., and Xu, H.: Close range photogrammetry for dynamically tracking drifted snow deposition, Cold Regions Science and Technology, 121, 141–153, https://doi.org/10.1016/j.coldregions.2015.08.013, 2016.

Bernard, E., Friedt, J. M., Tolle, F., Griselin, M., Marlin, C., and Prokop, A.: Investigating snowpack volumes and icing dynamics in the moraine of an Arctic catchment using UAV photogrammetry, The Photogrammetric Record, 32, 497–512, https://doi.org/10.1111/phor.12217, 2017.

Besl, P. J. and McKay, N. D.: Method for registration of 3-D shapes, pp. 586–606, Boston, MA, https://doi.org/10.1117/12.57955, 1992.

Bühler, Y., Marty, M., Egli, L., Veitinger, J., Jonas, T., Thee, P., and Ginzler, C.: Snow depth mapping in high-alpine catchments using digital photogrammetry, The Cryosphere, 9, 229–243, https://doi.org/10.5194/tc-9-229-2015, 2015.

Bühler, Y., Adams, M. S., Bösch, R., and Stoffel, A.: Mapping snow depth in alpine terrain with unmanned aerial systems (UASs): potential and limitations, The Cryosphere, 10, 1075–1088, https://doi.org/10.5194/tc-10-1075-2016, 2016.

Bühler, Y., Adams, M. S., Stoffel, A., and Boesch, R.: Photogrammetric reconstruction of homogenous snow surfaces in alpine terrain applying near-infrared UAS imagery, International Journal of Remote Sensing, 38, 3135–3158, https://doi.org/10.1080/01431161.2016.1275060, 2017.

Bühler, Y., Bebi, P., Christen, M., Margreth, S., Stoffel, L., Stoffel, A., Marty, C., Schmucki, G., Caviezel, A., Kühne, R., Wohlwend, S., and Bartelt, P.: Automated avalanche hazard indication mapping on a statewide scale, Natural Hazards and Earth System Sciences, 22, 1825–1843, https://doi.org/10.5194/nhess-22-1825-2022, publisher: Copernicus GmbH, 2022.

Bührle, L. J., Marty, M., Eberhard, L. A., Stoffel, A., Hafner, E. D., and Bühler, Y.: Spatially continuous snow depth mapping by aeroplane photogrammetry for annual peak of winter from 2017 to 2021 in open areas, The Cryosphere, 17, 3383–3408, https://doi.org/10.5194/tc-17-3383-2023, 2023.

Chen, Y. and Medioni, G.: Object modelling by registration of multiple range images, Image and Vision Computing, 10, 145–155, https://doi.org/10.1016/0262-8856(92)90066-C, 1992.

Deems, J. S., Painter, T. H., and Finnegan, D. C.: Lidar measurement of snow depth: a review, Journal of Glaciology, 59, 467–479, https://doi.org/10.3189/2013JoG12J154, 2013.

Deschamps-Berger, C., Gascoin, S., Berthier, E., Deems, J., Gutmann, E., Dehecq, A., Shean, D., and Dumont, M.: Snow depth mapping from stereo satellite imagery in mountainous terrain: evaluation using airborne laser-scanning data, The Cryosphere, 14, 2925–2940, https://doi.org/10.5194/tc-14-2925-2020, 2020.

Dharmadasa, V., Kinnard, C., and Baraër, M.: An Accuracy Assessment of Snow Depth Measurements in Agro-Forested Environments by UAV Lidar, Remote Sensing, 14, 1649, https://doi.org/10.3390/rs14071649, 2022.

Donager, J., Sankey, T. T., Sánchez Meador, A. J., Sankey, J. B., and Springer, A.: Integrating airborne and mobile lidar data with UAV photogrammetry for rapid assessment of changing forest snow depth and cover, Science of Remote Sensing, 4, 100 029, https://doi.org/10.1016/j.srs.2021.100029, 2021.

Dong, C. and Menzel, L.: Snow process monitoring in montane forests with time-lapse photography, Hydrological Processes, 31, 2872–2886, https://doi.org/10.1002/hyp.11229, 2017.

EAWS: Standards: Avalanche Problems, https://www.avalanches.org/standards/avalanche-problems/, 2024.

Eberhard, L. A., Sirguey, P., Miller, A., Marty, M., Schindler, K., Stoffel, A., and Bühler, Y.: Intercomparison of photogrammetric platforms for spatially continuous snow depth mapping, The Cryosphere, 15, 69–94, https://doi.org/10.5194/tc-15-69-2021, 2021.

Fey, C., Schattan, P., Helfricht, K., and Schöber, J.: A compilation of multitemporal TLS snow depth distribution maps at the Weisssee snow research site (Kaunertal, Austria), Water Resources Research, 55, 5154–5164, https://doi.org/10.1029/2019WR024788, 2019.

Filhol, S., Perret, A., Girod, L., Sutter, G., Schuler, T. V., and Burkhart, J. F.: Time-Lapse Photogrammetry of Distributed Snow Depth During Snowmelt, Water Resources Research, 55, 7916–7926, https://doi.org/10.1029/2018WR024530, 2019.

Garvelmann, J., Pohl, S., and Weiler, M.: From observation to the quantification of snow processes with a time-lapse camera network, Hydrology and Earth System Sciences, 17, 1415–1429, https://doi.org/10.5194/hess-17-1415-2013, 2013.

Goelles, T., Hammer, T., Muckenhuber, S., Schlager, B., Abermann, J., Bauer, C., Expósito Jiménez, V. J., Schöner, W., Schratter, M., Schrei, B., and Senger, K.: MOLISENS: MObile LIdar SENsor System to exploit the potential of small industrial lidar devices for geoscientific applications, Geoscientific Instrumentation, Methods and Data Systems, 11, 247–261, https://doi.org/10.5194/gi-11-247-2022, 2022.

Hancock, H., Prokop, A., Eckerstorfer, M., Borstad, C., and Hendrikx, J.: Monitoring cornice dynamics and associated avalanche activity with a terrestrial laser scanner, International Snow Science Workshop Proceedings 2018, Innsbruck, Austria, pp. 323–327, https://arc.lib.montana.edu/snow-science/item.php?id=2544, 2018a.

Hancock, H., Prokop, A., Eckerstorfer, M., and Hendrikx, J.: Combining high spatial resolution snow mapping and meteorological analyses to improve forecasting of destructive avalanches in Longyearbyen, Svalbard, Cold Regions Science and Technology, 154, 120–132, https://doi.org/10.1016/j.coldregions.2018.05.011, 2018b.

Hancock, H., Eckerstorfer, M., Prokop, A., and Hendrikx, J.: Quantifying seasonal cornice dynamics using a terrestrial laser scanner in Svalbard, Norway, Natural Hazards and Earth System Sciences, 20, 603–623, https://doi.org/10.5194/nhess-20-603-2020, 2020.

Harder, P., Schirmer, M., Pomeroy, J., and Helgason, W.: Accuracy of snow depth estimation in mountain and prairie environments by an unmanned aerial vehicle, The Cryosphere, 10, 2559–2571, https://doi.org/10.5194/tc-10-2559-2016, 2016.

Issler, D., Gisnås, K. G., Gauer, P., Glimsdal, S., Domaas, U., and Sverdrup-Thygeson, K.: Naksin – a New Approach to Snow Avalanche Hazard Indication Mapping in Norway, https://doi.org/10.2139/ssrn.4530311, 2023.

Jaakkola, A., Hyyppä, J., and Puttonen, E.: Measurement of Snow Depth Using a Low-Cost Mobile Laser Scanner, IEEE Geoscience and Remote Sensing Letters, 11, 587–591, https://doi.org/10.1109/LGRS.2013.2271861, 2014.

Jacobs, J. M., Hunsaker, A. G., Sullivan, F. B., Palace, M., Burakowski, E. A., Herrick, C., and Cho, E.: Snow depth mapping with unpiloted aerial system lidar observations: a case study in Durham, New Hampshire, United States, The Cryosphere, 15, 1485–1500, https://doi.org/10.5194/tc-15-1485-2021, 2021.

Kapper, K. L., Goelles, T., Muckenhuber, S., Trügler, A., Abermann, J., Schlager, B., Gaisberger, C., Eckerstorfer, M., Grahn, J., Malnes, E., Prokop, A., and Schöner, W.: Automated snow avalanche monitoring for Austria: State of the art and roadmap for future work, Frontiers in Remote Sensing, 4, https://www.frontiersin.org/articles/10.3389/frsen.2023.1156519, 2023.

Koenderink, J. J. and Doorn, A. J. v.: Affine structure from motion, JOSA A, 8, 377–385, https://doi.org/10.1364/JOSAA.8.000377, 1991.

Kopp, M., Tuo, Y., and Disse, M.: Fully automated snow depth measurements from time-lapse images applying a convolutional neural network, Science of The Total Environment, 697, 134 213, https://doi.org/10.1016/j.scitotenv.2019.134213, 2019.

Koutantou, K., Mazzotti, G., Brunner, P., Webster, C., and Jonas, T.: Exploring snow distribution dynamics in steep forested slopes with UAV-borne LiDAR, Cold Regions Science and Technology, 200, 103 587, https://doi.org/10.1016/j.coldregions.2022.103587, 2022.

Larson, K. M., Gutmann, E. D., Zavorotny, V. U., Braun, J. J., Williams, M. W., and Nievinski, F. G.: Can we measure snow depth with GPS receivers?, Geophysical Research Letters, 36, https://doi.org/10.1029/2009GL039430, 2009.

Lehning, M., Bartelt, P., Brown, B., Russi, T., Stöckli, U., and Zimmerli, M.: snowpack model calculations for avalanche warning based upon a new network of weather and snow stations, Cold Regions Science and Technology, 30, 145–157, https://doi.org/10.1016/S0165-232X(99)00022-1, 1999.

LeWinter, A. L., Finnegan, D. C., Hamilton, G. S., Stearns, L. A., and Gadomski, P. J.: Continuous Monitoring of Greenland Outlet Glaciers Using an Autonomous Terrestrial LiDAR Scanning System: Design, Development and Testing at Helheim Glacier, 2014, C31B–0292, https://ui.adsabs.harvard.edu/abs/2014AGUFM.C31B0292L, 2014.

Liu, J., Chen, R., Ding, Y., Han, C., and Ma, S.: Snow process monitoring using time-lapse structure-from-motion photogrammetry with a single camera, Cold Regions Science and Technology, 190, 103 355, https://doi.org/10.1016/j.coldregions.2021.103355, 2021.

Mallalieu, J., Carrivick, J. L., Quincey, D. J., Smith, M. W., and James, W. H. M.: An integrated Structure-from-Motion and time-lapse technique for quantifying ice-margin dynamics, Journal of Glaciology, 63, 937–949, https://doi.org/10.1017/jog.2017.48, 2017.

Marti, R., Gascoin, S., Berthier, E., de Pinel, M., Houet, T., and Laffly, D.: Mapping snow depth in open alpine terrain from stereo satellite imagery, The Cryosphere, 10, 1361–1380, https://doi.org/10.5194/tc-10-1361-2016, 2016.

Nolan, M., Larsen, C., and Sturm, M.: Mapping snow depth from manned aircraft on landscape scales at centimeter resolution using structure-from-motion photogrammetry, The Cryosphere, 9, 1445–1463, https://doi.org/10.5194/tc-9-1445-2015, 2015.

Prokop, A.: Assessing the applicability of terrestrial laser scanning for spatial snow depth measurements, Cold Regions Science and Technology, 54, 155–163, https://doi.org/10.1016/j.coldregions.2008.07.002, 2008.

Romanov, P., Tarpley, D., Gutman, G., and Carroll, T.: Mapping and monitoring of the snow cover fraction over North America, Journal of Geophysical Research: Atmospheres, 108, https://doi.org/10.1029/2002JD003142, 2003.

Schaer, P., Skaloud, J., Landtwing, S., and Legat, K.: Accuracy Estimation for Laser Point Cloud Including Scanning Geometry, in: Mobile Mapping Symposium 2007, Padova, 2007.

Schmid, L., Medic, T., Frey, O., and Wieser, A.: Target-based georeferencing of terrestrial radar images using TLS point clouds and multi-modal corner reflectors in geomonitoring applications, ISPRS Open Journal of Photogrammetry and Remote Sensing, 13, 100 074, https://doi.org/10.1016/j.ophoto.2024.100074, 2024.

Schweizer, J., Bruce Jamieson, J., and Schneebeli, M.: Snow avalanche formation, Reviews of Geophysics, 41, https://doi.org/10.1029/2002RG000123, 2003.

Shaw, T. E., Deschamps-Berger, C., Gascoin, S., and McPhee, J.: Monitoring Spatial and Temporal Differences in Andean Snow Depth Derived From Satellite Tri-Stereo Photogrammetry, Frontiers in Earth Science, 8, https://www.frontiersin.org/articles/10.3389/feart.2020.579142, 2020.

Vander Jagt, B., Lucieer, A., Wallace, L., Turner, D., and Durand, M.: Snow Depth Retrieval with UAS Using Photogrammetric Techniques, Geosciences, 5, 264–285, https://doi.org/10.3390/geosciences5030264, 2015.

Voordendag, A., Goger, B., Klug, C., Prinz, R., Rutzinger, M., Sauter, T., and Kaser, G.: Uncertainty assessment of a permanent long-range terrestrial laser scanning system for the quantification of snow dynamics on Hintereisferner (Austria), Frontiers in Earth Science, 11, https://www.frontiersin.org/articles/10.3389/feart.2023.1085416, 2023.

515

Voordendag, A. B., Goger, B., Klug, C., Prinz, R., Rutzinger, M., and Kaser, G.: AUTOMATED AND PERMANENT LONG-RANGE TERRESTRIAL LASER SCANNING IN A HIGH MOUNTAIN ENVIRONMENT: SETUP AND FIRST RESULTS, ISPRS Annals of the Photogrammetry, Remote Sensing and Spatial Information Sciences, V-2-2021, 153–160, https://doi.org/10.5194/isprs-annals-V-2-2021-153-2021, 2021.

520

Vuthea, V. and Toshiyoshi, H.: A Design of Risley Scanner for LiDAR Applications, in: 2018 International Conference on Optical MEMS and Nanophotonics (OMN), pp. 1–2, https://doi.org/10.1109/OMN.2018.8454641, 2018.

Warren, S. G.: Optical properties of snow, Reviews of Geophysics, 20, 67–89, https://doi.org/10.1029/RG020i001p00067, _eprint: https://onlinelibrary.wiley.com/doi/pdf/10.1029/RG020i001p00067, 1982.

Wiscombe, W. J. and Warren, S. G.: A Model for the Spectral Albedo of Snow. I: Pure Snow, Journal of the Atmospheric Sciences, 37,

525

2712–2733, https://doi.org/10.1175/1520-0469(1980)037<2712:AMFTSA>2.0.CO;2, 1980.

Zhou, Q.-Y., Park, J., and Koltun, V.: Open3D: A Modern Library for 3D Data Processing, https://doi.org/10.48550/arXiv.1801.09847, 2018.

Zweifel, B., Lucas, C., Hafner, E., Techel, F., Marty, C., and Stucki, T.: Schnee und Lawinen in den Schweizer Alpen. Hydrologisches Jahr 2018/19, https://www.dora.lib4ri.ch/wsl/islandora/object/wsl%3A22232/, 2019.